Title:

A novel noise reduction filter for improving visibility of early CT signs of hyperacute stroke: evaluation of the filter's performance–Preliminary clinical experience

Noriyuki Takahashi,[1] Yongbum Lee, PhD,[2] Du-Yih Tsai, PhD,[2] Kiyoshi Ishii, MD,[1]

[1]Department of Radiology, Sendai City Hospital,

[2]Department of Radiological Technology, School of Health Sciences, Niigata University,

The corresponding author:

Noriyuki Takahashi

Department of Radiology, Sendai City Hospital,

3-1, Shimizukouji, Wakabayashi-ku, Sendai, 984-0075, Japan

TEL: 81-22-266-7111(3661)

FAX: 81-22-211-8972

E-mail: norizaemon@pop02.odn.ne.jp

Type of manuscript:

Original article, Radiation physics

Title:

A novel noise reduction filter for improving visibility of early CT signs of hyperacute stroke: evaluation of the filter's performance–Preliminary clinical experience

Type of manuscript:

Original article, Radiation physics

Abstract

Purpose: To evaluate the performance of a novel noise reduction filter for improving the visibilty of early CT signs of hyperacute stroke on nonenhanced CT images.

Material and Methods: Fourteen patients with middle cerebral artery occlusion within 4.5 hours after onset were used for evaluations. Signal-to-noise ratio (SNR) of the processed images with the noise reduction filter and that of original images were measured. Moreover, two neuroradiologists visually rated all the processed and original images on the visibility of normal and abnormal gray-white matter interface.

Results: The SNR value of the processed images was approximately eight times as high as that of the original images, and a 87% reduction of noise was achieved using this technique. In the visual assessment, the results showed that both the visibility of normal gray-white matter interface and that of the loss of the gray-white matter interface were significantly improved by using the proposed method ($p<0.05$).

Conclusion: The noise reduction filter proposed in the present study has the potential to improve the visibility of early CT signs of hyperacute stroke on nonenhanced CT images.

Key word: Computed tomography, Infarction, Computer-applications, Adaptive smoothing filter

Introduction

Currently, computed tomography (CT) is still the most commonly used imaging modality in the diagnosis of hyperacute stroke because of its wide availability and examination speed, although the advanced magnetic resonance (MR) imaging is superior to the nonenhanced CT in respect of sensitivity in the detection of cerebral ischemia within the first few hours after symptom onset.[1,2] With the introduction of thrombolysis for acute stroke, much attention has been directed to identify early CT signs of cerebral ischemia on CT images over the last decade.[3-8] The early CT signs have been used as exclusion criteria for thrombolysis. However, because the detection of the early CT signs is considerably difficult, the detectability of the early CT signs is largely dependent on the skill and experiences of the readers.[9,10] Therefore, the improvement of detectability of the early CT signs for less experienced readers would have been desired.

The loss of gray-white matter interface which is one of the early CT signs is very subtle. The visibility of this sign is adversely affected by image noise on CT images.[11] To improve the visibility of the loss of gray-white matter interface, a soft-copy review with variable window width and center level settings has been performed.[12] By observation with narrow window width, the enhanced gray-white matter contrast can be obtained. However, this leads to a relative accentuation of image noise. Another way to improve the visibility of this subtle early CT sign is to use optimized CT acquisition protocols, such as tube current-time product, and reconstruction algorithms, so that the image noise can be reduced. However, the image noise could not be completely removed even by using this method.

One way to remove image noise is to apply image processing techniques such as filters to CT images. To deal with this issue, we have previously reported a noise reduction filter for improving visibility of early CT signs of hyperacute stroke.[13] In this report, instead of clinical CT images, only computer-simulated gray-white matter phantom images were used for the filter performance study. The experiments indicated that the proposed filter was able to reduce image noise while preserving the interface of computer-simulated gray-white matter phantom images.

The present paper is a significant extension of our previous work. The purpose of this study was to quantitatively and qualitatively evaluate the performance of our previously proposed filter for the improvement of visibility of early CT signs on nonenhanced CT images. As a more adequate expression of our proposed filter, in the present paper we rename the filter as the adaptive partial averaging filter (APAF).

Materials and Methods

Description of the APAF processing technique

The main feature of the APAF is that the use of the method can enhance image data by removing noise without significantly blurring the structures in the image. The APAF is a specially designed filter used to perform local smoothing using a variable filter size and shape. When determining the filter size and shape, a thresholding for image binarization is necessary. The approach to thresholding employed in the APAF partly refers to a report related to adaptive neighborhood contrast enhancement.[14] Fig. 1 shows the flow chart of the main steps of the proposed method. The main steps are as follows.

(1) After applying a $M \times M$ averaging filter to the original image, each pixel (i,j) of the image I is assigned an upper window $W_{max} \times W_{max}$ centered on it whose size is smaller than the original image, where W_{max} is an odd number.

(2) Let T be a given threshold. Pixel (k,l) within $W_{max} \times W_{max}$ is assigned a binary mask value 1 if $|I(k,l) - I(i,j)| \leq T$, else it is assigned a binary mask value 0. This results in constructing a binary image. Fig. 2 shows an example in the case of T=5 and W_{max} = 9.

(3) For each window size $C \times C$ (C=3, 5,…., W_{max}), the percentage P_0 of zeros is computed over the region of external area of $C \times C$ window. The actual window size (W) is determined when the percentage P_0 is not greater than α%, and is closest to α%. Fig. 2(c) shows three various external areas (C=3, 7, 9) and the respective P_0 computed from each window. W=7

was determined as the actual window size, when α was set at 60.

(4) The processed image I' is obtained from $I'(i, j) = M(i, j)$, where $M(i, j)$ is the mean value in the image I of pixels labeled as the binary mask value 1 in the window $W \times W$ around pixel (i,j). Fig. 2(d) shows final mask image obtained from Fig. 2(b) and Fig. 2(c).

(5) Steps (2)~(4) are iteratively performed at each pixel as center pixel in the original image.

The performance of the APAF for noise reduction largely depends on the parameters T and α. The parameters are mainly used to determine the filter size and shape. In particular, T is used to determine the filter shape by perceiving the boundary of an object (*e.g.*, normal gray-white matter interface) in a region of interest. The filter size and shape vary according to the pixel value distribution of the object around a center pixel. For example, if pixels of edges (e.g. normal gray-white matter interface) are included in a region of interest, a small filter size is used as a weak low-pass filter to preserve the edge of the anatomical structure. If none of edges is included in a region of interest, a large filter size (maximum filter size, 13×13) is used as a powerful low-pass filter to smooth the noisy images. The filter determined by these parameters includes only object pixels, which correspond to the pixels assigned the binary mask value 1 in Fig. 2(d), distinguished from background pixels in a region of interest.

In the present study, the optimal parameters for brain CT images, T=3.0, α = 60%, W_{max} = 13 and M = 5 were used. These parameters were obtained from the performance evaluation using computer-simulated images in our previous studies .[13]

Patients and Imaging

The study protocol was approved by the institutional review board. Informed consent was not required. As the preliminary trial, the study protocol was applied to consecutive 14 patients with hyperacute MCA-territory infarction. No patients with old cerebral infarction were included in this selection. All images showed subtle loss of the gray-white matter interface in the insular

ribbon and/or in the lentiform nucleus. All images were proved to be MCA-territory infarctions by diffusion-weighted magnetic resonance (MR) imaging or by follow-up CT (1-7 days after the onset of symptoms). Early CT signs of 14 patients in the present study are summarized in Table 1. The mean age of the patients studied was 72 years (age range, 50-90 years). The mean interval between onset of stroke ictus and the first imaging was 2 hours 47 minutes (range, 1 hour to 4.5 hours). The CT examination of entire brain was performed using ProSeed Accell (GE Yokogawa Medical systems, Tokyo, Japan) in sequential mode with 5 mm contiguous sections for infratentorial region and 10 mm contiguous sections for supratentorial region. The images were reconstructed with a standard-version reconstruction algorithm routinely set in our institution. Axial CT images through basal ganglia regions were selected, which were retrieved from our picture archiving and communication system (PACS) workstation (PathSpeed^{TM}; GE yokogawa Medical systems, Tokyo, Japan). The CT images selected were obtained with matrix size of 512×512, slice thickness 10 mm, tube voltage 120 kV, tube current-time product 400 mAs and field of view 250 mm. The image data in Digital Imaging and Communications in Medicine (DICOM) version 3.0 format were transferred to a personal computer (n9030; HP, Tokyo, Japan). The CT values were transformed to real numbers from integral numbers for executing processing. Therefore, the format of the processed image data was original-file one. The pixel depth was 16 bits. The APAF was applied to each image of the 14 cases. As a result, fourteen APAF-processed images and 14 original images were obtained.

Performance evaluation

To quantitatively evaluate the performance of the APAF for noise reduction, the signal-to-noise ratio (SNR) was calculated. The SNR was computed by dividing the mean pixel value in a region of interest (ROI) by the standard deviation (SD) of the pixel values in the ROI. The ROI with a size of 10×10 pixels covering the area of the lentiform nucleus of normal cerebral

hemisphere on each image was selected. We calculated the SNR of each image of 14 cases, as well as the mean values of the SNRs of the original and the processed images.

To validate improvement in visibility of the loss of the gray-white differentiation using the APAF, a visual assessment of the images of the 14 cases was performed. Two board-certified neuroradiologists including one author (K.I.) who selected all the cases, reviewed both the original and the processed images of fourteen cases with variable window widths and center level settings on a 20-inch color monitor (Multiscan G500: SONY, Tokyo, Japan). In this test, 20-HU window width was used. The readers were aware of the focal parenchymal areas of hypoattenuation on the images in each case. Both readers independently graded all the images about the visibility of

(a) Normal gray-white matter interface in the lentiform nucleus and the insular ribbon in normal hemisphere,

(b) The loss of gray-white matter interface in the lentiform nucleus and/or the cortical ribbon in the region of stroke.

A grading was conducted with a five-point Likert scale (1, not evaluated; 2, inadequate; 3, adequate; 4, good; 5, excellent). Data obtained from this grading process were presented as mean ± standard deviation. The data were analyzed using the Wilcoxon's signed rank test. Interobserver agreement was measured by using Spearman's rank test.

Results

On visual inspection the APAF-processed images showed significant reduction in image noise without blurring of normal gray-white matter interface. Examples of nonenhanced CT images of hyperacute stroke after applying the APAF is shown in Figs.3 and 4. Although the hypodense lesion can be discerned on the original image with very narrow window width, but processed images can provide more differentiation of subtle abnormality. The processed image is also

displayed with narrow window width (20 HU). This enables us to easily recognize accentuated gray-white matter contrast without enhancing image noise on the processed images.

Our measurement results showed that the mean SNR value of the original images and that of the processed images with the APAF were 17.4 (SD=2.6) and 133.9 (SD=59.1), respectively. The SNR value of the processed images was approximately eight times as high as that of the original images. The mean SD value of the ROIs of processed images with the APAF was 0.3 HU and that of the original images was 2.2 HU. Consequently, a 87% reduction of noise was obtained using the APAF. As mentioned earlier in this paper, one of the features of the proposed filter is that image noise can be significantly reduced, while the HU values of gray and white matters of the processed images remain almost unchanged as compared to the original ones. Thus, the extent of improvement in the contrast-to-noise ratio is similar to the SNR.

In the visual assessment on the normal gray-white matter interface, the mean score of the original images and that of the processed image were 2.50±0.39 and 4.36±0.41, respectively. Regarding the visibility of the loss of the gray-white matter interface, the mean score of the original images was 2.57±0.51 and that of the processed image was 4.54±0.41. Fig. 5 shows the results from two evaluations. The scores of all 14 processed images were higher than those of the original images in the two evaluations. Moreover, significant differences ($p < 0.05$) were found between the original images and the processed images in the two evaluations. The correlation coefficient of interobserver agreement was rho=0.44–0.75 ($p < 0.05$), representing fair to good interobserver agreement. The results showed that both the visibility of normal gray-white matter interface and that of the loss of the gray-white matter interface were significantly improved by using the APAF.

Discussion

In the diagnosis of hyperacute stroke, interobserver agreement for the detecting of parenchymal hypoattenuation is generally poor; it has been reported that the κ values for hypoattenuation

were ranged from 0.30 to 0.53.[9] One of the reasons for poor κ values for hypoattenuation may be subtle change of the attenuation in Hounsfield units in ischemic brain tissue. Kucinski et al reported a decrease of 1.3 HU at 2.5 hours after the onset of acute ischemic stroke.[15] Thus, removing image noise has an effect on detecting the subtle change of the attenuation in hyperacute stroke. In the visual assessment, both the visibility of the normal gray-white matter interface and that of the loss of the gray-white matter interface were improved by using the APAF in all 14 cases. This result might suggest that the normal gray-white matter interface was more conspicuous by using the APAF, so that the loss of the gray-white matter interface of hyperacute stroke was markedly enhanced.

Experienced readers interpreting stroke CT scans may detect all the early CT signs in the 14 cases used in this study. However, less-experienced readers may miss them, because the detectability of early CT signs is largely dependent on the skill and experiences of the readers.[9,10] Therefore, we believe that the APAF can help, in particular, less- experienced readers detect early CT sign at emergency institutions.

Image noise is one of the most important factors influencing the detectability of low-contrast objects, such as the hypoattenuation of ischemic brain parenchyma.[11] The use of higher tube current at CT scan is effective for reducing image noise. Another way to reduce image noise is use of reconstruction algorithms for smoothing.[16] However, it is difficult to substantially reduce image noise on CT images using these techniques.

The APAF is a kind of a smoothing filter. Therefore, the use of APAF would slightly blur detailed structures, such as normal gray-white matter interface on brain CT images. Nevertheless, the visibility of the normal gray-white matter interface is, as a whole, improved by using the APAF. This may be due to the great reduction of image noise although some blurring of edges of anatomical structures occurs. It was noted that the visual information shown on the APAF-processed images was somewhat different from that shown on the original CT images. Therefore, when using the APAF in clinical practice, the readers are recommended to

review both the standard CT images and the APAF-processed images for interpretation.

Reviewing a CT image with narrow window width on a monitor to accentuate the gray-white matter leads to an increase of sensitivity for the detection of early CT signs. However, this also leads to an increase of image noise. As a result, the interface between gray and white matter may be difficult to clearly identify as shown in Fig. 3. Our experimental results showed that by employing the APAF to the CT images, gray-white matter contrast was enhanced without accentuating the image noise when using a narrow window width. As shown in Figs. 3 and 4, the interfaces between gray and white matters can clearly recognize when viewing the APAF-processed images.

Noise reduction filters are generally used in two ways in CT scans: (1) directly applied to raw data for image reconstruction, (2) applied to reconstructed images. The former has the difficulty in obtaining the raw data from a CT scanner by general users. The latter can easily obtain the reconstructed images in DICOM format. Therefore, we adopted the latter in order to give priority to widespread the availability of our proposed method in the setting of clinical use. In addition, the execution time required for image data transfer implementation, image processing and image display with a personal computer was less than a minute. The widespread availability and the prompt response of the APAF could be advantageous in the diagnosis of hyperacute stroke in many emergency rooms.

The present study has limitations. First, no patients with old cerebral infarction were included in this study. In practice, patients with old cerebral infarction may be examined at emergency CT scans. More elaborate study on evaluating the visibility of early CT signs on images with old cerebral infarction is still required. Second, the performance evaluation was not conducted by employing a smoothing reconstruction algorithm recommended for the detection of early CT signs, because this reconstruction algorithm was not routinely set in our institution. In fact, standard-version reconstruction filters are generally used in most emergency rooms for examining not only hyperacute stroke but also another disorder. Thus, we believe that the

performance evaluation with standard CT images is of importance as an initial experiment. Further study on the performance evaluation with CT images obtained from optimized reconstruction algorithm would be necessary.

Furthermore, there is a possibility that false positive findings may occur by using the proposed image-processing technique. However, since only abnormal cases were used in the present study, we did not investigate this possibility. In the future, we plan to validate our approach on a larger set of images including both normal and abnormal cases. Also we will evaluate the diagnosis accuracy using receiver operating characteristic analysis.

In conclusion, the APAF has the potential to improve the visibility of early CT signs of hyperacute stroke on nonenhanced CT images.

Acknowledgement

The authors are grateful to Toshibumi Kinoshita, MD, for his participation in performance assessment as an observer. This study was supported in part by the Telecommunications Advancement Foundation (TAF) Japan.

References

1) Adams H, Adams R, del Zoppo G, Goldstein LB. Guidelines for the early management of patients with ischemic stroke: 2005 guidelines update a scientific statement from the Stroke Council of the American Heart Association/American Stroke Association. Stroke 2005;36:916-23.2
2) Adams HP Jr, Adams RJ, Brott T, del Zoppo GJ, Furlan A, Goldstein LB, et al. Guidelines for the early management of patients with ischemic stroke: A scientific statement from the Stroke Council of the American Stroke Association. Stroke 2003;34:1056-83.1
3) Balbel PA, Demchuk AM, Zhang J, Buchan AM. Validity and reliability of a quantitative computed tomography score in predicting outcome of hyperacute stroke before thrombolytic therapy. ASPECTS Study Group. Alberta Stroke Programme Early CT Score. Lancet 2000;355:1670-4.7
4) Provenzale JM, Jahan R, Naidich TP, Fox AJ. Assessment of the patient with hyperacute stroke: imaging and therapy. Radiology 2003;229:347-59.8
5) Tomura N, Uemura K, Inugami A, Fujita H, Higano S, Shishido F. Early CT findings in cerebral infarction: obscuration of the lentiform nucleus. Radiology 1988;168:463-7.3
6) Truwit CL, Barkovich AJ, Gean-Marton, Hibri N, Norman D. Loss of the insular ribbon: another early CT sign of acute middle cerebral artery infarction. Radiology 1990;176:801-6.4
7) von Kummer R, Allen KL, Holle R, Bozzao L, Bastianello S, Manelfe C, et al. Acute stroke: usefulness of early CT findings before thrombolytic therapy. Radiology 1997;205:327-33.5
8) Wardlaw JM, Dorman PJ, Lewis SC, Sandercock PA. Can stroke physicians and neuroradiologists identify signs of early cerebral infarction on CT? J Neurol Neurosurg Psychiatry 1999;67:651-3. 6
9) Wardlaw JM, Mielke O. Early signs of brain infarction at CT: observer reliability and

outcome after Thrombolytic treatment-systematic review. Radiology 2005;235:444-53.10

10) Schriger DL, Karafut M, Starkman S, Krueger M. Cranial computed tomography interpretation in acute stroke: physician accuracy in determining eligibility for thrombolytic therapy. JAMA 1998;279:1293-7.9

11) Tanaka C, Ueguchi T, Shimosegawa E, Sasaki N, Johkoh T, Nakamura H, et al. Effect of CT acquisition parameters in the detection of subtle hypoattenuation in acute cerebral infarction: a phantom study. Am J Neuroradiol 2006;27:40-5.11

12) Lev MH, Farkas J, Gemmete JJ, Hossain ST, Hunter GJ, Koroshetz WL, et al. Acute stroke: improved nonenhanced CT detection-benefits of soft-copy interpretation by using variable window width and center level settings. Radiology 1999;213:150-5.12

13) Takahashi N, Lee Y, Tsai DY, Ishii K, Kamio S. Improvement in visibility and detectability of early sign of acute stroke in nonenhanced CT images by using an adaptive partial smoothing filter. Nippon Hoshasen Gijutsu Gakkai Zasshi 2005;61:1531-41.18

14) Guis VH, Adel M, Rasigni M, R Georges. Adaptive neighborhood contrast enhancement in mammographic phantom images. Opt. Eng 2003;42:357-66. 15

15) Kucinski T, Vaterlein O, Glauche V, Fiefler J, Klotz E, Eckert B, et al. Correlation of apparent diffusion coefficient and computed tomography density in acute ischemic stroke. Stroke 2002;33:1786-91.16

16) Kalender WA. Computed Tomography: Fundamentals, System Technology, Image Quality, Applications. Munich: Publicis MCD Verlag, 2001. p. 85.

Figure captions

Fig.1. Flow chart of the main steps of the proposed method.

Fig.2. Adaptive neighborhood selection with a threshold value of T=5.

(a) An example of window image (I) whose initial window size is 9×9 (W_{max}=9). The pixel value of the central pixel in I is 35 [$I(i, j)$=35 (black)].

(b) Mask image generated from (a) in the case of T=5. For example, the pixel value $I(i, j)$ = 33 (gray: immediately above the central pixel) is assigned a binary mask value 1, because $|I(k, l)–I(i, j)|\leq T$ (i.e., |33-35|≤5).

(c) Determination of actual window size (W). The percentage of zeros (P_0) is computed over the region of external area (gray) of mask image with window size C=3, 7, 9. The actual window size is assigned as W=7, when P_0 is set at 60%.

(d) Final mask image obtained from (b) and (c). The processed image I' is obtained from $I'(i, j) = M(i, j)$, where $M(i, j)$ is the mean value in the image I of pixels labeled as the binary mask value 1 in the window $W \times W$ around pixel (i,j).

Fig. 3. A 50-year-old-man presented with right hemiplegia at 4 hours after stroke onset (Table 1, patient No 10).

A: The original image with the standard window width of 80HU shows that the loss of the gray-white matter interface of the left lenticular nucleus is barely identified.

B: The loss of the gray-white matter interface (arrows) becomes apparent when the original Image is displayed with a narrow window width of 20HU to accentuate the gray-white matter interface. However, image noise is markedly increased.

C: The APAF processed image viewed with a narrow window width of 20HU, shows that the visibility of the normal gray-white matter interface in the right cerebral hemisphere was greatly improved, and the loss of the gray-white matter interface of posterior part of the left lentiform

nucleus (arrows) is clearly detectable. Note that the image noise is unremarkable in spite of the narrow window width.

D: Diffusion-weighted MR image taken after the first CT scan demonstrates infarction in left MCA distribution (arrows).

Fig. 4. A 67-year-man with right hemiplegia at 4 hours after stroke onset (Table1, patient No 12).

A: The original image with the standard window width of 80HU shows that the loss of the gray-white matter interface of acute stroke is hardly detectable.

B: The original image with a narrow window width of 20HU shows that the loss of the gray-white matter interface of the left insular ribbon and frontal operculum is barely detectable (arrows).

C: The APAF-processed image viewed with a window width of 20HU shows that the loss of the gray-white matter interface of the left insular ribbon and frontal operculum is clearly visible (arrows).

D: Diffusion-weighted MR image taken after the first CT scan demonstrates hyperintensity representing cerebral infarction in left MCA distribution.

Fig.5. The scores given by two readers.

A: Visibility of normal gray-white matter interface observed by reader 1.

B: Visibility of normal gray-white matter interface observed by reader 2.

C: Visibility of the loss of gray-white matter interface observed by reader 1.

D: Visibility of the loss of gray-white matter interface observed by reader 2. Shaded bars represent the scores for the original images. Hatched bars represent the increase in the scores for the APAF-processed images.

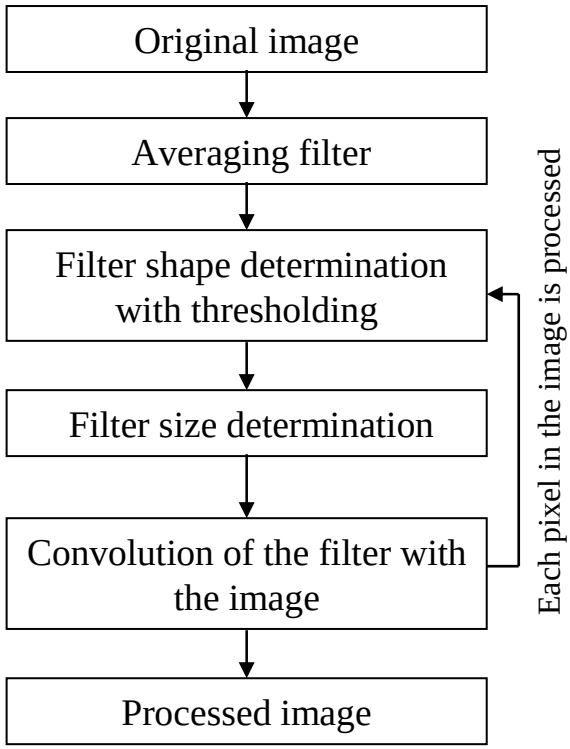
Original image
Averaging filter
Filter shape determination with thresholding
Filter size determination
Convolution of the filter with the image
Processed image
Each pixel in the image is processed

Fig. 1

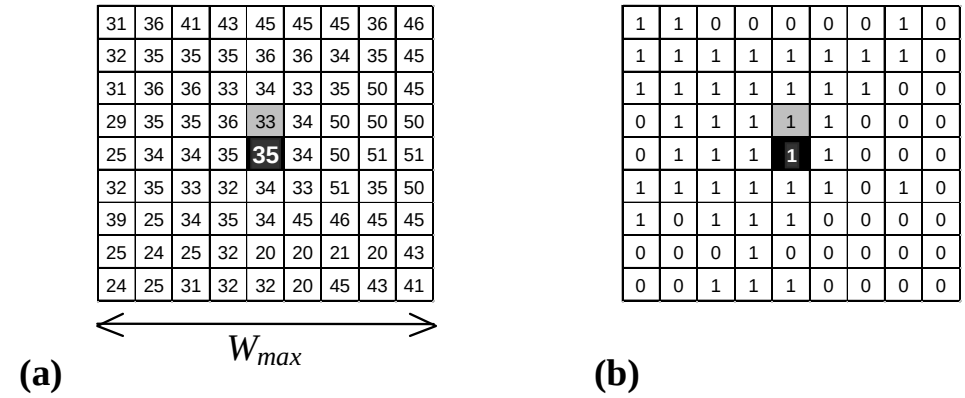
31 36 41 43 45 45 45 36 46
32 35 35 35 36 36 34 35 45
31 36 36 33 34 33 35 50 45
29 35 35 36 33 34 50 50 50
25 34 34 35 35 34 50 51 51
32 35 33 32 34 33 51 35 50
39 25 34 35 34 45 46 45 45
25 24 25 32 20 20 21 20 43
24 25 31 32 32 20 45 43 41
W_{max}
(a)
1 1 0 0 0 0 0 1 0
1 1 1 1 1 1 1 1 0
1 1 1 1 1 1 1 0 0
0 1 1 1 1 1 0 0 0
0 1 1 1 1 1 0 0 0
1 1 1 1 1 1 0 1 0
1 0 1 1 1 0 0 0 0
0 0 0 1 0 0 0 0 0
0 0 1 1 1 0 0 0 0
(b)
C=3
P_0 =0%
C=7
P_0 =45.8%
C=9
P_0 =68.7 (>60%)
(c)
(d)

Fig. 2

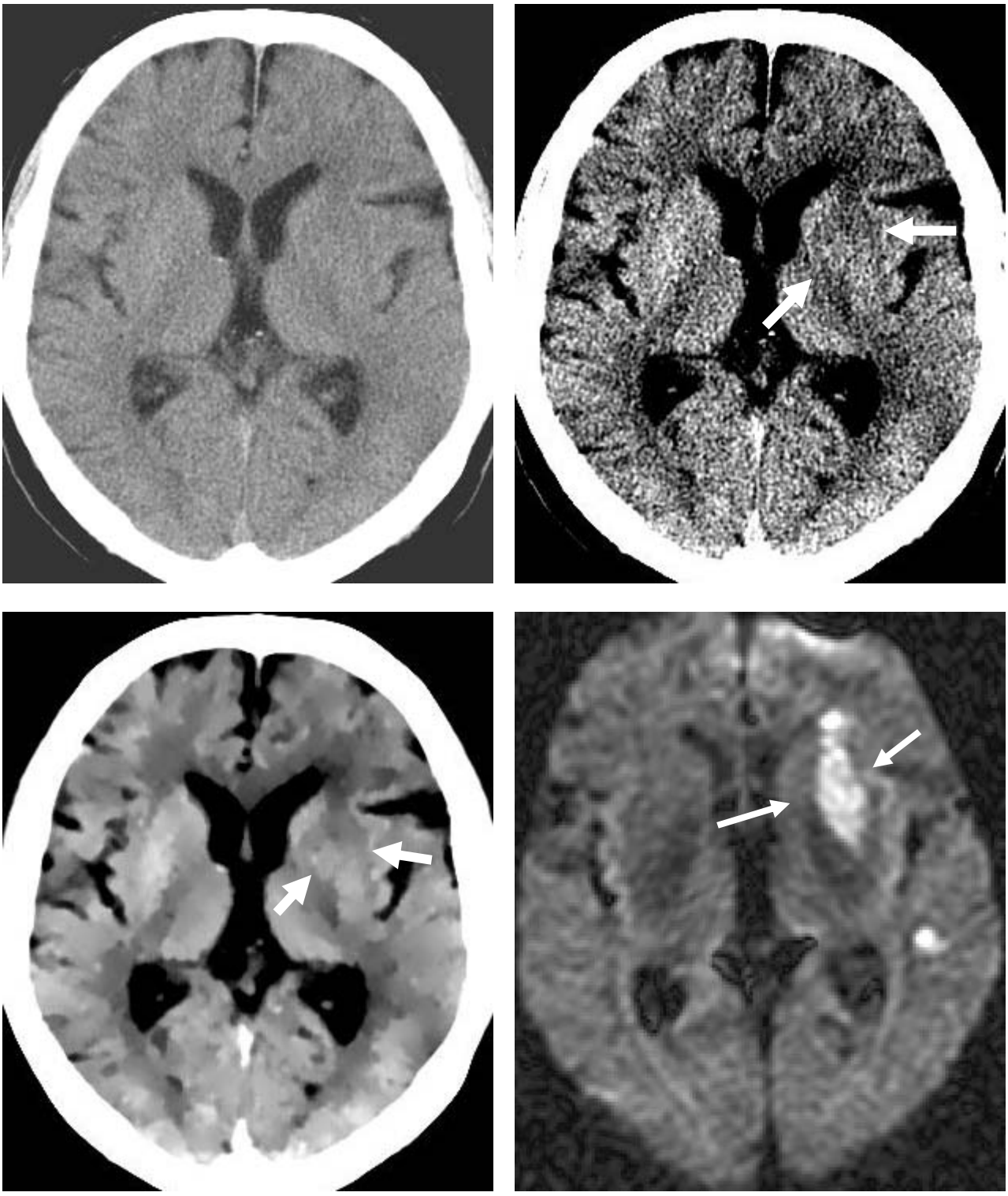

A	B
C	D

Fig. 3

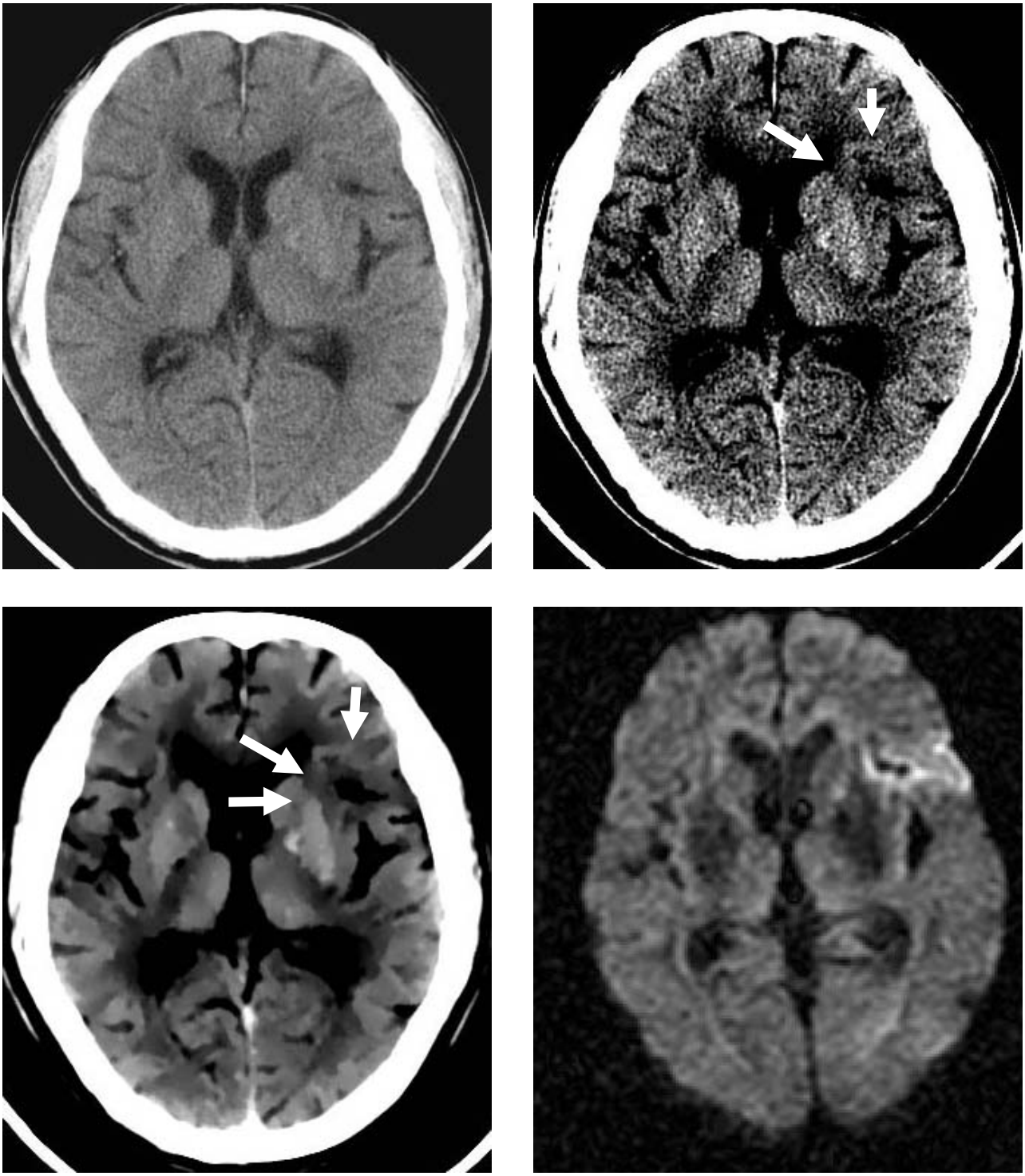

A	B
C	D

Fig. 4

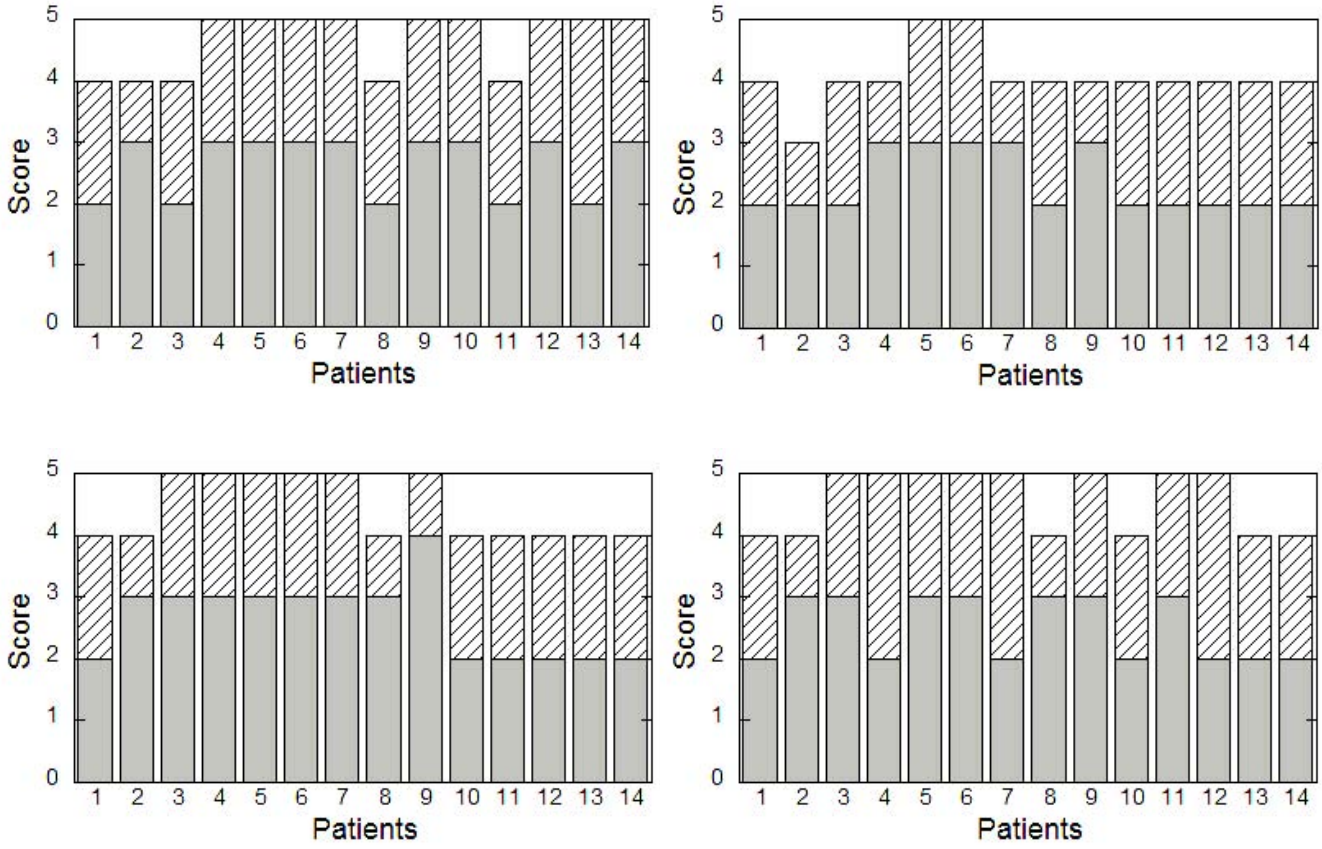

A	B
C	D

Fig. 5

Table 1. Summary of patients

Patient No.	Age (y)	Sex	Location of CT sign	Time to CT (h)
1	67	Male	Left PDLN	4.5
2	71	Male	Right LCR	4.5
3	90	Female	Right LCR	1.8
4	69	Female	Left PDLN, LCR	1.0
5	63	Female	Left PDLN, LCR	1.5
6	83	Male	Left OOLN, LCR	1.5
7	83	Female	Left OOLN, LCR	2.3
8	82	Female	Right LCR	1.7
9	75	Female	Left LCR	4.0
10	50	Male	Left PDLN	4.0
11	60	Male	Left LCR	3.0
12	67	Male	Left LCR	4.0
13	57	Male	Left PDLN, LCR	1.7
14	88	Female	Left PDLN, LCR	1.5

OOLN = obscured outline of lentiform nucleus

PDLN = partial disappearance of lentiform nucleus

LCR = loss of cortical ribbon

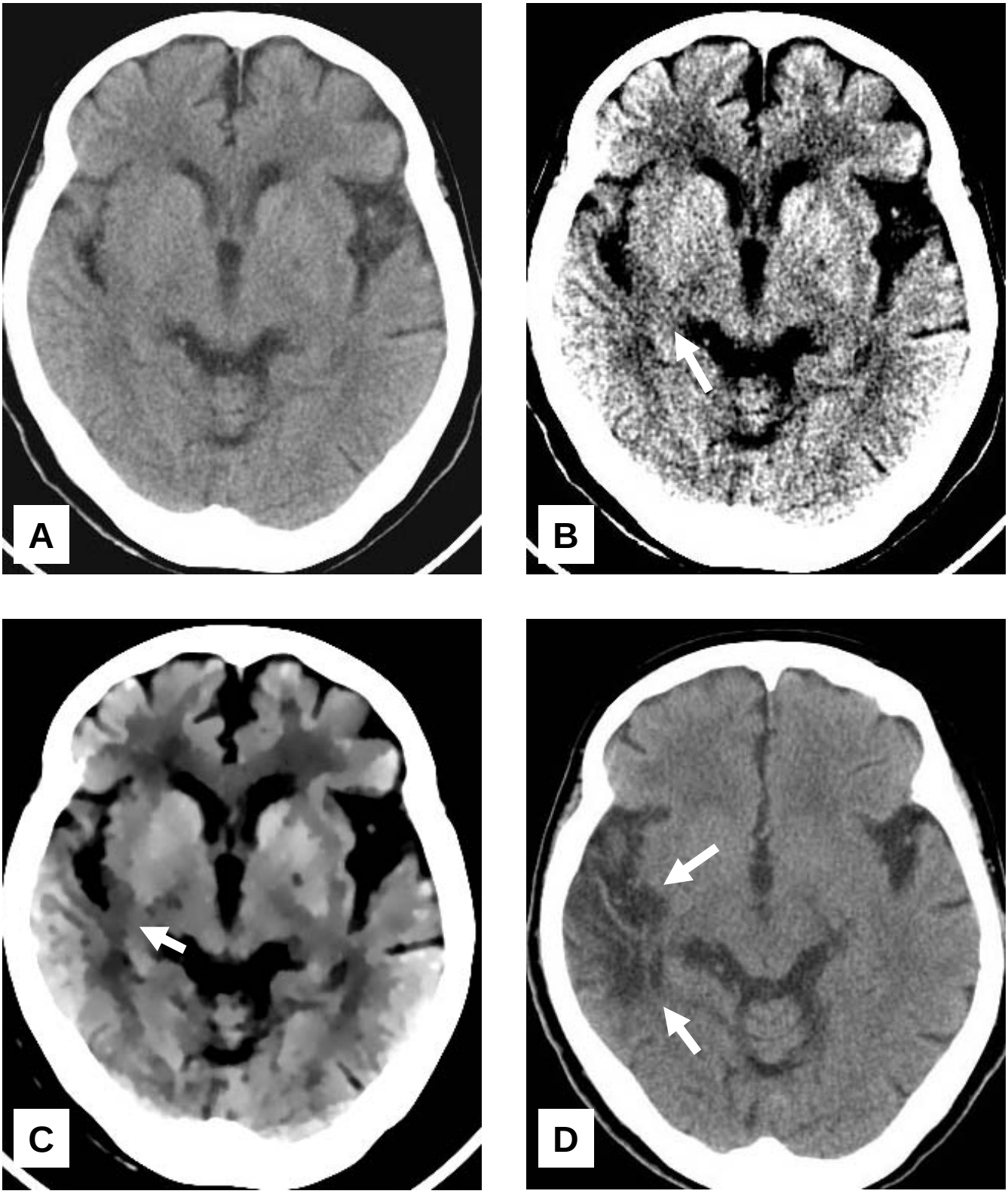
A
B
C
D